Food Chemistry: X 21 (2024) 101174

Contents lists available at ScienceDirect

Food Chemistry: X

journal homepage: www.sciencedirect.com/journal/food-chemistry-x

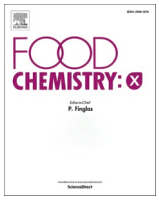

Mechanism of thermal oxidation into volatile compounds from (E)-4-decenal: A density functional theory study

Binchen Wang [a,b], Shaohua Dou [c], Shang Wang [d], Yi Wang [d], Sufang Zhang [a,b], Xinping Lin [a,b], Yingxi Chen [a,b], Chaofan Ji [a,b], Yiwei Dai [a,b], Liang Dong [a,b,*]

[a] School of Food Science and Technology, Dalian Polytechnic University, Dalian 116034, Liaoning, China
[b] National Engineering Research Centre of Seafood, Dalian 116034, Liaoning, China
[c] College of Life and Health, Dalian University, Dalian 116622, Liaoning, China
[d] School of Biotechnology, Dalian Polytechnic University, Dalian 116034, Liaoning, China

ARTICLE INFO

Keywords:
Unsaturated aldehyde
Theoretical calculation
Flavor
Oxidation mechanism

ABSTRACT

Unsaturated aliphatic aldehyde oxidation plays a significant role in the deep oxidation of fatty acids to produce volatile chemicals. Exposing the oxidation process of unsaturated aliphatic aldehydes is crucial to completely comprehend how food flavor forms. In this study, thermal desorption cryo-trapping in conjunction with gas chromatography-mass spectrometry was used to examine the volatile profile of (E)-4-decenal during heating, and 32 volatile compounds in all were detected and identified. Meanwhile, density functional theory (DFT) calculations were used, and 43 reactions were obtained in the 24 pathways, which were summarized into the peroxide reaction mechanism (ROOH), the peroxyl radical reaction mechanism (ROO·) and the alkoxy radical reaction mechanism (RO·). Moreover, the priority of these three oxidative mechanisms was the RO· mechanism > ROOH mechanism > ROO· mechanism. Furthermore, the DFT results and experimental results agreed well, and the oxidative mechanism of (E)-4-decenal was finally illuminated.

Introduction

Lipid oxidation during heating is one of the most important sources of flavor in food (Calín-Sánchez & Carbonell-Barrachina, 2021; Stier, 2000). Among these volatile compounds, unsaturated ten-carbon aliphatic aldehyde are important substances, such as decanal, (E)-2-decenal and (E)-4-decenal, etc (Angela & Andreas, 2010; Porter, Caldwell, & Mills, 1995; Zaldman, Klsillev, & Sasson, 1988). And (E)-4-decenal is a main unsaturated ten-carbons flavor compound generated in the lipid oxidative process with pineapple aroma, which is also an important part of food flavor formation. It is one of the common volatile flavor substances in the oxidation of cooking oil, and is often used as a high-end flavor in the food industry (Peng, Lan, & Lin, 2017). In our previous experiments, we found that unsaturated ten-carbons aldehydes can be further oxidized to produce shorter carbon-chain volatiles, which are the major components of the deep oxidation of fatty acids (Frankel, 1983; Wang, Zhang, & Lin, 2023). But their oxidative mechanisms are still unclear. Therefore, the in-depth analysis of the thermal oxidation mechanism of (E)-4-decenal is of great significance for the assembly and reduction of the real oleic acid oxidation process and food flavor formation reaction. At the same time, a full understanding of thermal oxidation mechanism of unsaturated aliphatic aldehyde to volatile substances can provide a theoretical basis for the precise regulation of flavor substances in the process of food hot processing, so as to realize the manual intervention and precise regulation of flavor in the food processing, and finally achieve the purpose of improving and enhancing the quality of food flavor.

It is found that the double bonds of unsaturated aldehydes could readily absorb energy during heating, leading to the breaking of the hydrocarbon bond of α-C and the formation of olefin and hydrogen radicals (Al-Otaibi, Mahmoud, & Almuqrin, 2021; Balan & Rajakumar, 2018; Santacesaria, Sorrentino, & Rainone, 2000; Sheridan, 1946). Olefin radical, as one of the important intermediates of oxidation reaction, could combine with oxygen or peroxyl hydroxyl radicals to form peroxyl oxygen radicals or peroxide. These free radicals may be further oxidized and degraded during heating to generate volatiles with shorter carbon chains.

Theoretical chemistry is an effective approach to study chemical

* Corresponding author at: School of Food Science and Technology, National Engineering Research Centre of Seafood, Dalian Polytechnic University, Qinggongyuan Road No.1, Dalian 116034, China.
E-mail address: dongliang@dlpu.edu.cn (L. Dong).

https://doi.org/10.1016/j.fochx.2024.101174
Received 15 June 2023; Received in revised form 31 January 2024; Accepted 1 February 2024
Available online 6 February 2024

Table 1
Volatile substances produced during heating of (E)-4-decenal.

No.	Compounds	RI	identification method	Content(μg/mg)					
				60 °C	90 °C	120 °C	150 °C	180 °C	210 °C
Alkanes									
1	(E)-3-nonene	886	RI, MS	0.30 ± 0.03^{b}	0.37 ± 0.11^{ab}	0.22 ± 0.18^{b}	0.90 ± 0.63^{ab}	1.42 ± 0.38^{a}	0.81 ± 0.37^{ab}
2	2-nonene	902	RI, MS	nd	nd	nd	0.04 ± 0.02^{a}	nd	nd
3	(E)-1,3-nonadiene	924	RI, MS	nd	nd	nd	nd	0.16 ± 0.05^{a}	0.10 ± 0.04^{a}
Aldehydes									
4	(E)-4-decenal	1198	RI, MS, STD	330.01 ± 174.51^{a}	274.19 ± 39.81^{a}	199.96 ± 71.25^{a}	199.31 ± 22.48^{a}	167.14 ± 8.23^{a}	223.69 ± 112.37^{a}
5	(Z)-4-decenal	1193	RI, MS, STD	0.33 ± 0.29^{a}	0.44 ± 0.39^{a}	0.45 ± 0.38^{a}	0.48 ± 0.32^{a}	0.72 ± 0.30^{a}	nd
6	(E, E)-2,4-decadienal	1317	RI, MS, STD	0.20 ± 0.13^{a}	0.53 ± 0.41^{a}	0.68 ± 0.17^{a}	0.46 ± 0.13^{a}	nd	nd
7	Hexanal	800	RI, MS, STD	nd	0.21 ± 0.11^{bc}	0.22 ± 0.14^{bc}	0.49 ± 0.21^{a}	0.54 ± 0.14^{ab}	0.39 ± 0.15^{ab}
8	(E)-2-heptenal	958	RI, MS, STD	nd	0.07 ± 0.04^{bc}	0.10 ± 0.07^{abc}	0.14 ± 0.08^{abc}	0.41 ± 0.17^{a}	0.16 ± 0.04^{ab}
9	(E)-2-octenal	1060	RI, MS, STD	nd	nd	0.21 ± 0.08^{a}	0.23 ± 0.11^{a}	0.51 ± 0.14^{a}	0.34 ± 0.10^{a}
Alcohols									
10	1-octen-3-ol	980	RI, MS, STD	0.13 ± 0.03^{a}	0.18 ± 0.08^{a}	0.20 ± 0.05^{a}	0.16 ± 0.12^{a}	0.46 ± 0.20^{a}	0.12 ± 0.01^{a}
11	(E)-3-nonen-1-ol	1143	RI, MS, STD	0.30 ± 0.16^{a}	nd	nd	nd	nd	nd
12	(E)-2-decenol	1257	RI, MS, STD	nd	0.76 ± 0.41^{a}	0.36 ± 0.20^{ab}	0.68 ± 0.55^{a}	nd	nd
13	(E)-3-decen-1-ol	1232	RI, MS	nd	nd	0.32 ± 0.10^{a}	nd	0.58 ± 0.10^{a}	nd
14	Dec-4-en-1-ol	1257	RI, MS	nd	nd	nd	nd	nd	2.44 ± 1.72^{a}
15	(E)-2-dodecen-1-ol	1478	RI, MS	nd	nd	0.30 ± 0.10^{a}	0.08 ± 0.06^{b}	nd	nd
16	2,4-decadien-1-ol	1264	RI, MS	nd	nd	nd	0.49 ± 0.45^{a}	nd	nd
Ketones									
17	3-nonen-2-one	1142	RI, MS, STD	nd	nd	nd	0.25 ± 0.12^{a}	0.46 ± 0.12^{a}	0.45 ± 0.26^{a}
Acids									
18	Hexanoic acid	990	RI, MS, STD	0.12 ± 0.06^{ab}	0.18 ± 0.14^{a}	nd	nd	nd	nd
19	(E)-4-decenoic acid	1366	RI, MS, STD	14.98 ± 3.80^{b}	29.37 ± 9.38^{a}	71.54 ± 3.90^{a}	12.63 ± 4.97^{b}	27.50 ± 9.77^{b}	8.29 ± 2.18^{b}
20	Valeric acid	903	RI, MS, STD	nd	nd	nd	nd	0.08 ± 0.02^{a}	nd
21	(E)-2-decenoic acid	1392	RI, MS, STD	nd	nd	0.53 ± 0.14^{a}	nd	nd	nd
Esters									
22	Ethyl palmitate	1974	RI, MS	0.02 ± 0.01^{a}	nd	nd	nd	nd	0.02 ± 0.01^{a}
23	Isopropyl palmitate	2023	RI, MS	0.05 ± 0.00^{b}	0.35 ± 0.23^{a}	nd	nd	nd	nd
24	γ-decalactone	1470	RI, MS	nd	nd	1.27 ± 0.47^{a}	0.26 ± 0.13^{bc}	0.84 ± 0.31^{ab}	nd
25	Methyl tuberate	1502	RI, MS, STD	nd	nd	nd	0.11 ± 0.03^{a}	0.24 ± 0.10^{a}	nd
26	Ethyl hexanoate	1000	RI, MS, STD	nd	nd	nd	nd	nd	0.16 ± 0.09^{a}
Others									
27	2-pentylfuran	993	RI, MS	0.33 ± 0.06^{a}	0.49 ± 0.32^{a}	nd	nd	nd	nd
28	Pentylbenzene	1157	RI, MS	0.02 ± 0.00^{a}	0.13 ± 0.06^{a}	0.09 ± 0.04^{a}	0.05 ± 0.01^{a}	0.08 ± 0.01^{a}	0.20 ± 0.15^{a}
29	Naphthalene	1182	RI, MS	0.24 ± 0.07a	0.27 ± 0.04^{a}	0.62 ± 0.31^{a}	0.18 ± 0.17^{a}	0.51 ± 0.18^{a}	0.32 ± 0.11^{a}
30	1-(1-ethoxyethoxy)-butane	872	RI, MS	0.03 ± 0.01^{abc}	0.03 ± 0.02^{abc}	0.04 ± 0.01^{bc}	nd	0.08 ± 0.02^{ab}	0.07 ± 0.04^{a}
31	1,1′-[ethylidenebis(oxy)] bis-butane	1094	RI, MS	0.47 ± 0.12^{b}	0.57 ± 0.15^{ab}	1.17 ± 0.73^{ab}	0.90 ± 0.14^{a}	0.95 ± 0.17^{ab}	nd
32	1,1-diethoxyhexane	1092	RI, MS	0.01 ± 0.00^{b}	0.03 ± 0.01^{b}	nd	nd	nd	0.08 ± 0.03^{a}

Nd = Compound not detected in the sample. MS = Identification by MS spectra, RI = Kovat's retention indexes, STD = Comparison with a standard compound; The content was the average of three replicates ± standard deviation. "a, b, c," indicated significant difference ($P < 0.05$).

reaction mechanisms, which has been widely used in many fields in recent years (Borges, Colby, & Das, 2021; Hammes-Schiffer, 2017). In theoretical chemistry, one of the most common methods is density functional theory (DFT) (Verma and Truhlar, 2020; Hine Nicholas and Hine, 2016). It can calculate the molecular structure, reaction parameters, transition states and products during chemical reactions. Meanwhile, it can also determine the active sites of functional groups, the activation energy and reaction rate constant of the reaction, which provided the data basis for the kinetic study of the thermal oxidation process by comparing the reaction barrier and the rate constant (Grambow, Pattanaik, & Green, 2020). Therefore, the application of density functional theory to the field of flavor chemistry can deeply elucidate the molecular formation mechanism of food flavor.

In this study the volatile forming mechanism of (E)-4-decenal thermal oxidation was examined by using DFT calculations and experimental data. The volatile compounds generated from the oxidation of (E)-4-decenal during heating were firstly investigated. Then, DFT calculations were used to deeply explore the mechanism of (E)-4-decenal thermal oxidation. By comparing and analyzing the potential energy surface and rate constant of each reaction, the priority of each reaction path was finally determined. Thus, the oxidation mechanism of (E)−4-decenal was finally elucidated.

Materials and methods

Chemicals

Standard chemicals: analytical grade ((E)-4-decenal, 2, 4, 6-trimethyl-pyridine, and C4-C20 alkanes, etc) were purchased from Aladdin (Shanghai, China).

Experimental method

Extraction and collection of volatile compounds from (E)-4-decenal during heating was performed by using a thermal desorption cryo-trapping system, with a qualified microchamber/thermal extractor (M−CTE250 Markes International, UK). (E)-4-decenal was diluted to 100 μL/mL, 20 μL of the sample was taken and 10 μL of diluted cyclohexanone (2 μg/mL) was added as a quantitative internal standard. An Agilent 6890/5975C GC–MS system (Santa Clara, CA, USA) equipped with an HP-5 ms column (30 m × 0.25 mm i.d., 0.25 μm film thickness; J&W Scientific) was used for the analysis of volatile compounds desorbed from the sample (Chai, Li, & Zhang, 2019; Drabova, Tomaniova, & Kalachova, 2013; Dymerski, 2017; Jeleń, Majcher, & Dziadas, 2012; Peter, Giorgia, & Mariarosa, 2016). Specific parameters from the experiments are detailed in the Supplementary Material.

Computational methods

In this study, all the reaction mechanism and related structures were calculated on Gussian16 software package (Becke, 1992, 1993; Elroby, Banaser, & Aziz, 2022; Fukui, 1981; Shabani, Latina, & Li, 2020; Yang & Lee., 1986). The Gibbs free energy was calculated by Shermo 2.0.8 program, and the accurate reaction potential energy surface was obtained (Albaugh, Boateng, & Bradshaw, 2016; Mahmoud, Shiroudi, & Abdel-Rahman, 2020; Ryu, Park, & KiM, 2018; Tian & Chen, 2021). The TST calculator could be used to calculate reaction rate constants (Tian Lu, http://sobereva.com/310). The Condensed Fukui Function (CFF) of molecular structure was calculated using the Multiwfn (Tian & Chen, 2012).

Calculation of molecular orbital

The Chemcraft was used to determine the charge density of each atom in the molecule. The VMD charting application was used to obtain the molecular orbital diagram (Humphrey, Dalke, & Schulten, 1996).

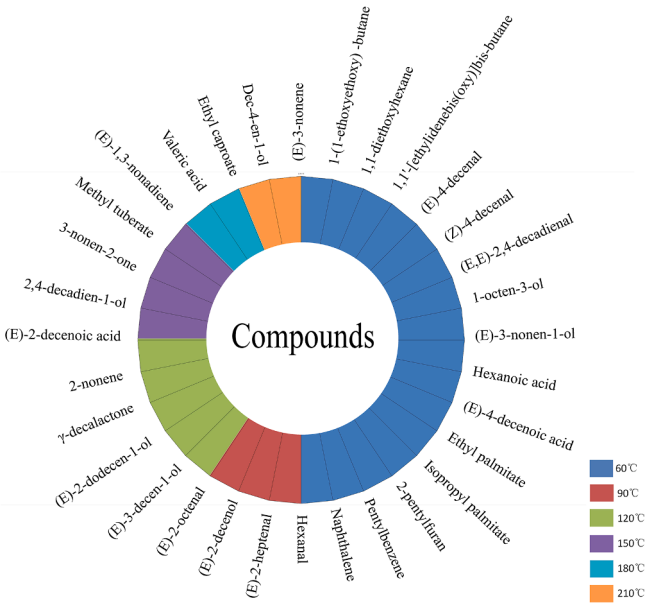

Fig. 1. Temperature of volatile chemicals are produced during the thermal oxidation of (E)-4-decenal.

Statistical analysis

There were three duplicates of each experiment. The measured data were expressed as mean ± standard deviation. SPSS 18.0 (Chicago, IL, USA) statistical software was used to analyze the significance among relevant samples at 0.05 ($P < 0.05$) level by one-way ANOVA.

Results and discussion

Characterization of volatile substances produced by (E)-4-decenal during heating

As shown in Table 1, a total of 32 volatile compounds were identified from (E)-4-decenal oxidation during heating. Meanwhile, Fig. 1 visualises the volatile composition of each temperature point during heating. As shown in Fig. 1, a total of 16 volatiles were detected at 60℃, accounting one half of the total volatiles throughout the whole heating process. Most of them have a good flavor, such as 1-octen-3-ol with its strong mushroom odor and hexanoic acid with the cheese odor (Ama, Fb, & Db, 2019). It can be inferred that the (E)-4-decenal oxidation could take place at lower temperatures, and its oxidative products contribute more to the flavor production.

As the temperature increased, 3 and 5 new volatile compounds were produced at 90℃ and 120℃ respectively, including two unsaturated aldehydes and some alcohols (Fig. 1), such as (E)-2-heptenal, (E)-2-octenal and (E)-2-decenol. The presence of longer carbon chains products, such as ethyl palmitate and methyl tuberate, could be attributed to the etherification between oxidative pyrolysis product. At 180℃, the relative contents of some volatile products increased significantly, such as (E)-2-heptenal, (E)-2-octenal, 1-octen-3-ol. They are common volatile substances with good flavor in food. As the temperature continued to rise to 210℃, the relative content of some volatiles showed a decreasing trend, and more volatiles with shorter carbon chains were generated. At the same time, (E)-1,3-nonadiene began to form at this temperature.

Mechanism of (E)-4-decenal theomal oxidation based on DFT calculations

As shown in Fig. 2, 43 reactions were obtained in thermal oxidation process of (E)-4-decenal by using DFT calculations. These 43 reactions were summarized into the peroxyl radical (ROO·) mechanism, the

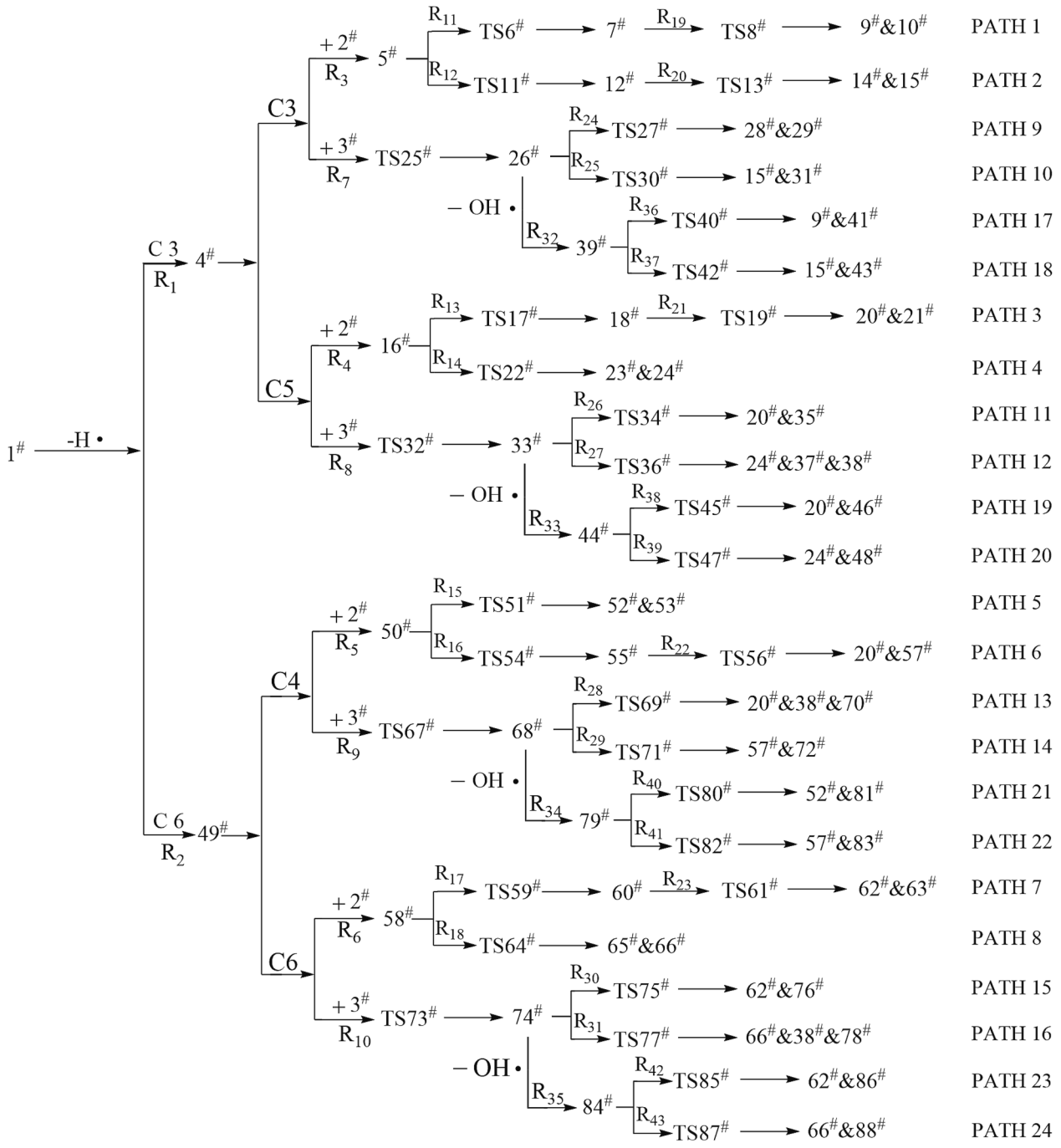

Fig. 2. Diagram for the whole oxidation of (E)-4-decenal.

peroxyl (ROOH) mechanism and the alkoxy radical (RO·) mechanism. Fig. 3 displayed the molecular structures of reactants, transition states, intermediates, and end products that were involved in each reaction. Besides, Fig. 4 showed each thermal oxidative decomposition pathways of (E)-4-decenal.

Analysis of peroxyl radical mechanism (ROO·) in (E)-4-decenal thermal oxidation

As shown in Fig. 4, in the initial stage of oxidation of (E)-4-decenal, the H atom on the α-C (C3, C6) of the carbon–carbon double bond is so reactive that the C—H bond can easily absorb energy and break, forming the corresponding olefinic and hydrogen radicals. Then, electrons could rearrange on the C3, C4, C5 sites or C4, C5, C6 sites to form a π conjugated system. This system could continue to oxidized with oxygen or peroxide (Li and Josef, 1996). Therefore, when oxygen attacks C3 or C5 site of the π conjugated system (C3-C4-C5), the olefinic peroxide radical 3-ROO· (R_3, $5^{\#}$) or 5-ROO· (R_4, $16^{\#}$) are formed, respectively. While oxygen attacks C4 or C6 site of the π conjugated system (C4-C5-C6), the olefinic peroxide radical 4-ROO· (R_5, $50^{\#}$) or 6-ROO· (R_6, $58^{\#}$) are formed, respectively.

As 3-ROO·, 4-ROO·, 5-ROO· and 6-ROO· olefinic peroxide radicals are more active, they could attack the adjacent carbon atom leading to further cleavage of the carbon chain into smaller molecules (Path 1–8). It can be seen from the Fig. 4 (Path 1 and Path 2), the O—O· of 3-ROO· ($5^{\#}$) would attack the C2 or C4 site to form intermediate products ($7^{\#}$ or $12^{\#}$) via transition state $TS6^{\#}$ or $TS11^{\#}$. Then, the single bond between C2-C3 or C3-C4 breaks via the $TS8^{\#}$ (R_{19}) or $TS13^{\#}$ (R_{20}) to form the

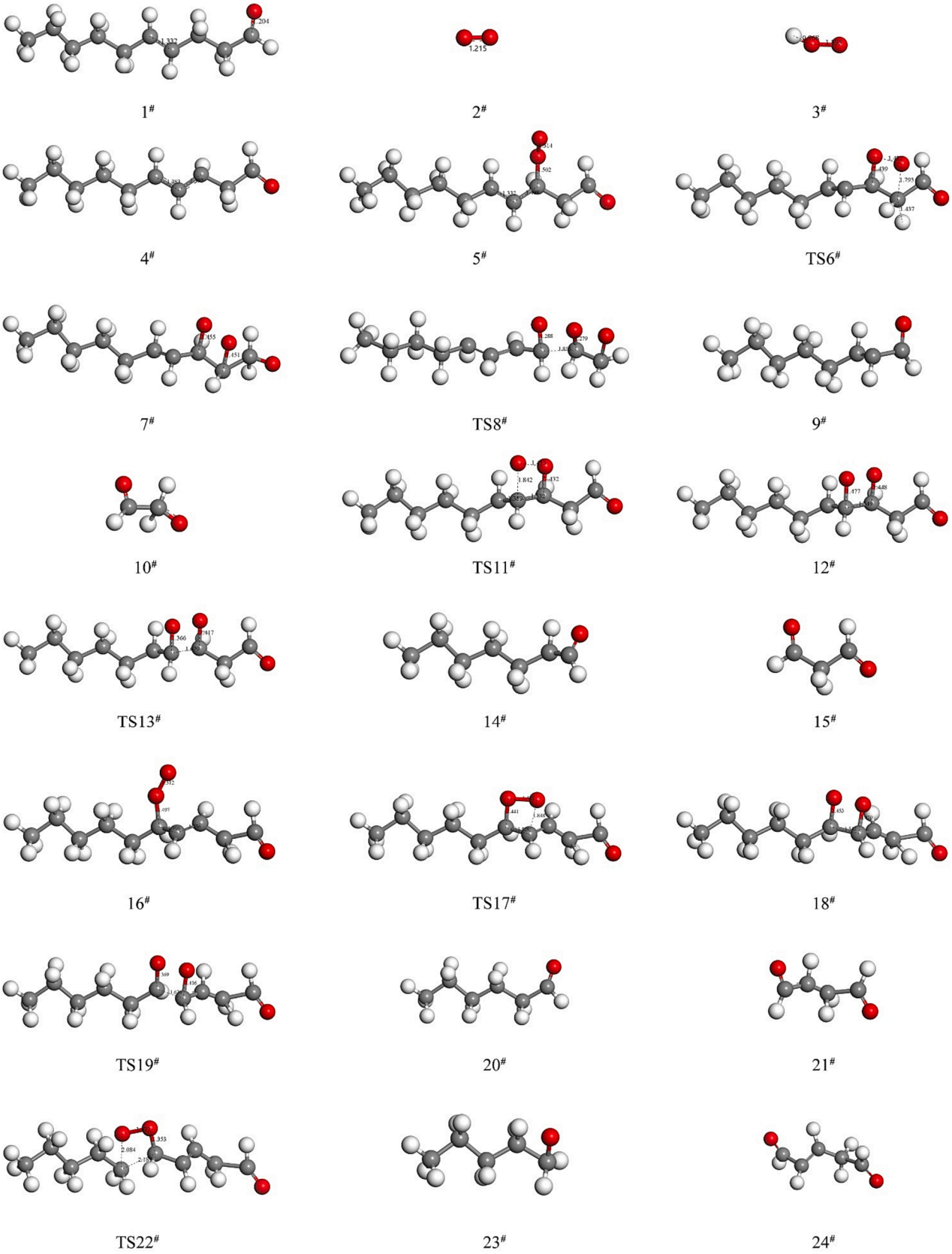

Fig. 3. The composition of the compounds involved in the oxidation of (E)-4-decenal.

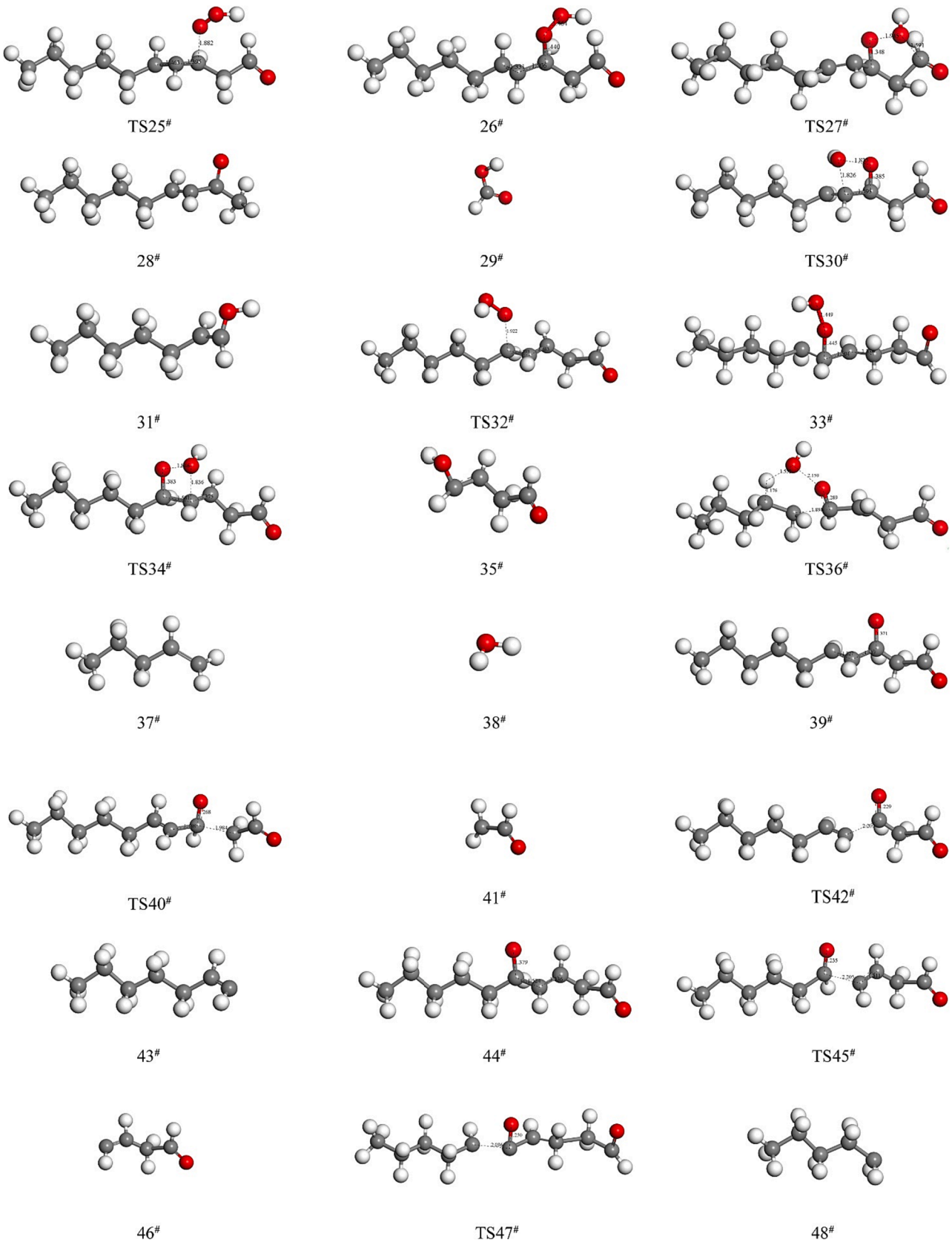

Fig. 3. (*continued*).

final products (9#&10#): 2-octenal and $CHOCH_2O\cdot$ (Path 1) or the final products (14#&15#): $CH_3(CH_2)_5\dot{C}HCHO$ and malondialdehyde (Path 2), respectively.

The further oxidation of the 4-ROO·, 5-ROO· and 6-ROO· follows a similar pathway as above. With the O—O· of the 4-ROO· attacking C3, 2-heptenal and $C\dot{O}(CH_2)_2CHO$ (52#&53#, Path 5) are formed via TS51#. If

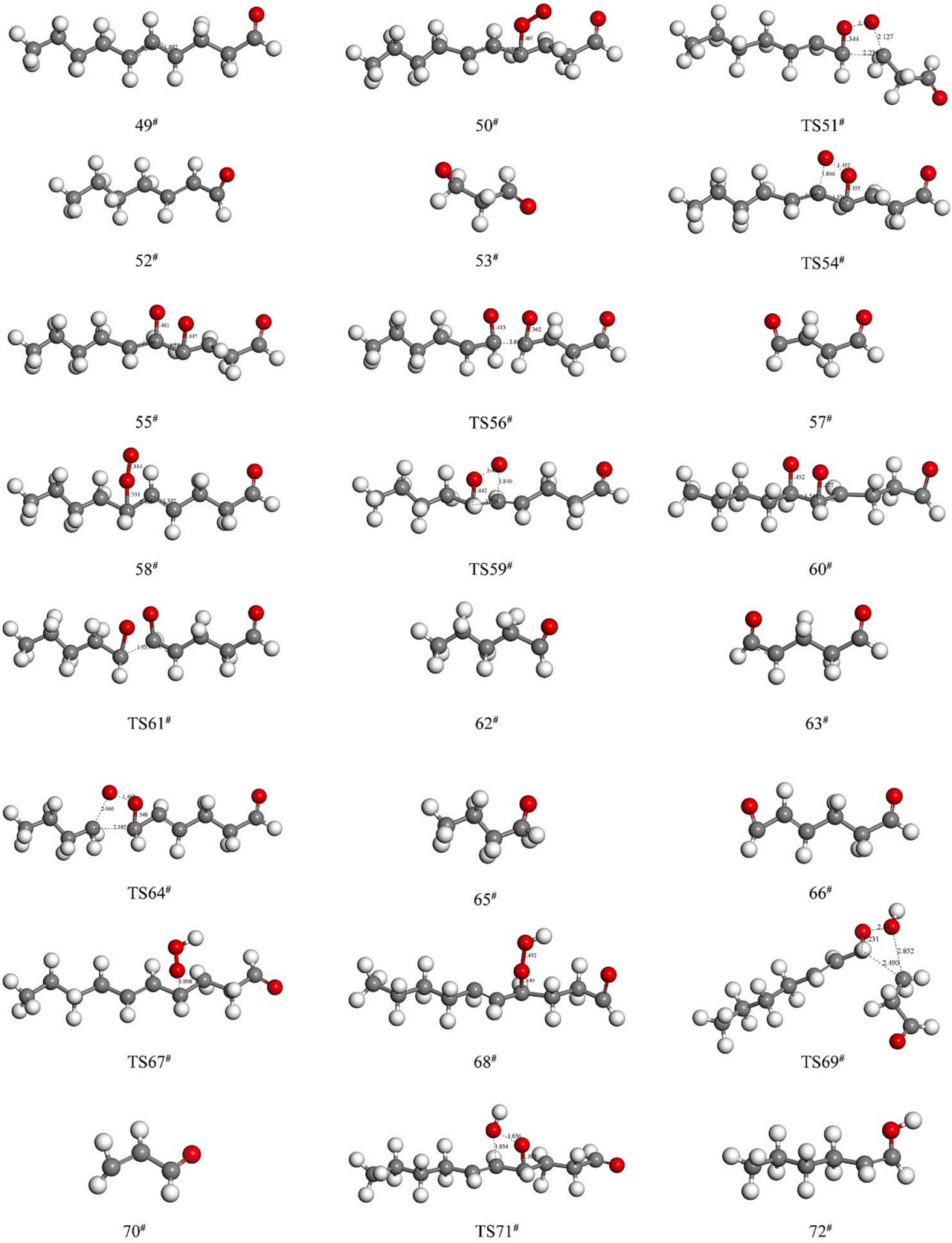

Fig. 3. (*continued*).

C5 is selected, the intermediate product $55^{\#}$ is firstly formed via $TS54^{\#}$, then final products hexanal and succinaldehyde are formed via R_{16} and R_{22} ($20^{\#}$&$57^{\#}$, Path 6). When the O—O· of the 5-ROO· attacks the C4 site to form the intermediate product $18^{\#}$ via $TS17^{\#}$ (R_{13}), then hexanal and $CHOCH_2CHCHO$· are formed via $TS19^{\#}$ ($20^{\#}$&$21^{\#}$, Path 3). And the O—O· of the 5-ROO· could also attack C6 to form the final products:

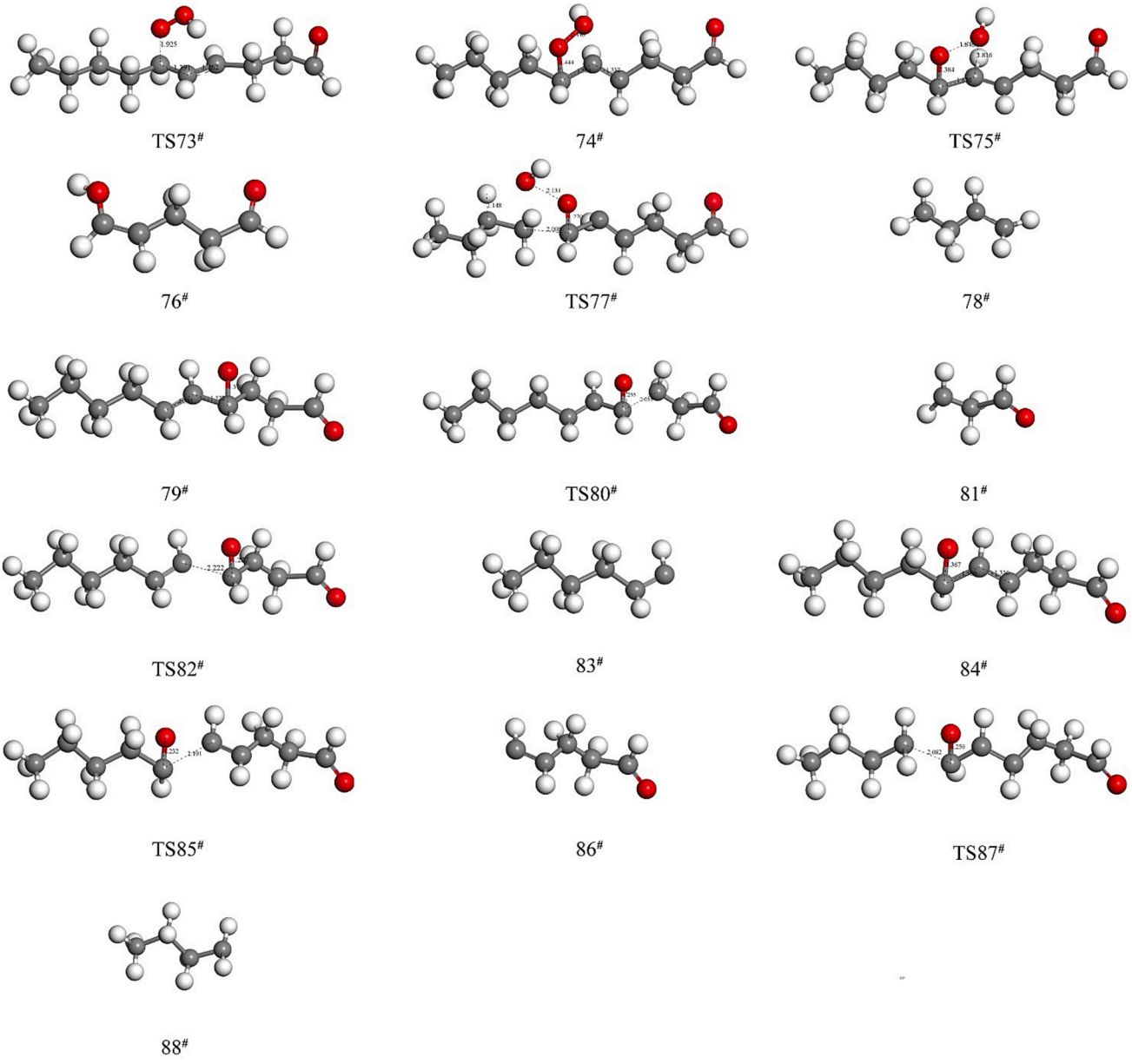

Fig. 3. (*continued*).

$CH_3(CH_2)_3CH_2O$· and 2-alkenyl glutaraldehyde ($23^{\#}$&$24^{\#}$, Path 4). For 6-ROO·olefinic peroxide radicals, if the C5 site is selected, the intermediate product $60^{\#}$ was firstly formed via $TS59^{\#}$ (R_{13}), then pentanal and $CHOCH(CH_2)_2CHO$ are generated via $TS61^{\#}$ ($62^{\#}$&$63^{\#}$, Path 7). While, if the C7 site is selected, $CH_3(CH_2)_2CH_2O$·and 2-alkenyl adipaldehyde ($65^{\#}$&$66^{\#}$, Path 8) are generated.

Analysis of peroxide reaction mechanism (ROOH) in (E)-4-decenal thermal oxidation

During the heating process, oxygen can react with hydrogen radical to form peroxy hydroxyl radicals (OOH·, $3^{\#}$). This radical could continue to attack the π conjugated system (C3-C4-C5 or C4-C5-C6). When OOH· attacks C3-C4-C5 system, 3-ROOH or 5-ROOH are formed via transition states ($TS25^{\#}$or $TS32^{\#}$) respectively. While OOH· attacks C4-C5-C6 conjugated system, 4-ROOH or 5-ROOH are formed via $TS67^{\#}$ or $TS73^{\#}$. These peroxides (3-ROOH, 4-ROOH, 5-ROOH and 6-ROOH) are unstable and will further oxidize. As shown in Fig. 4 (Path 9 and Path 10), the hydroxyl group in the peroxyl group of 3-ROOH will attack adjacent carbon atoms C2 or C4. In order to determine which carbon is more active, the molecular orbitals are plotted using Fukui function calculations. As shown in Fig. 5, the density of the electron cloud is expressed in terms of chromaticity, with darker colours indicating a higher density of electron clouds in the region and more active reactions (Charles and Sebens., 2021; Ryu et al., 2018). It can be seen clearly from the Fig. 5 that the closer to the aldehyde group, the darker the color becomes. This is due to the electron absorption effect of the aldehyde group resulting in a relatively high density of electron clouds on its neighbour atoms. As a result, when the hydroxyl group approaches the C2, the hydroxyl group connects to C1 is more active, which leads to the hydrogen on C3 transfers to C2 and the C2-C3 bond breaks simultaneously (R_{24}) to form the final product: 3-nonen-2-one and formic acid via $TS27^{\#}$ ($28^{\#}$&$29^{\#}$, path 9). However, if the hydroxyl group is close to C4, the C3-C4 single bond will be broken directly via the $TS30^{\#}$ (R_{25}) to form the final products: 2-hepten-1-ol and malondialdehyde ($15^{\#}$&$31^{\#}$, Path 10).

Similarly, the hydroxyl group of the 4-ROOH attached to C3 is abstracted to form a water molecule, then the C3-C4 bond is broken via

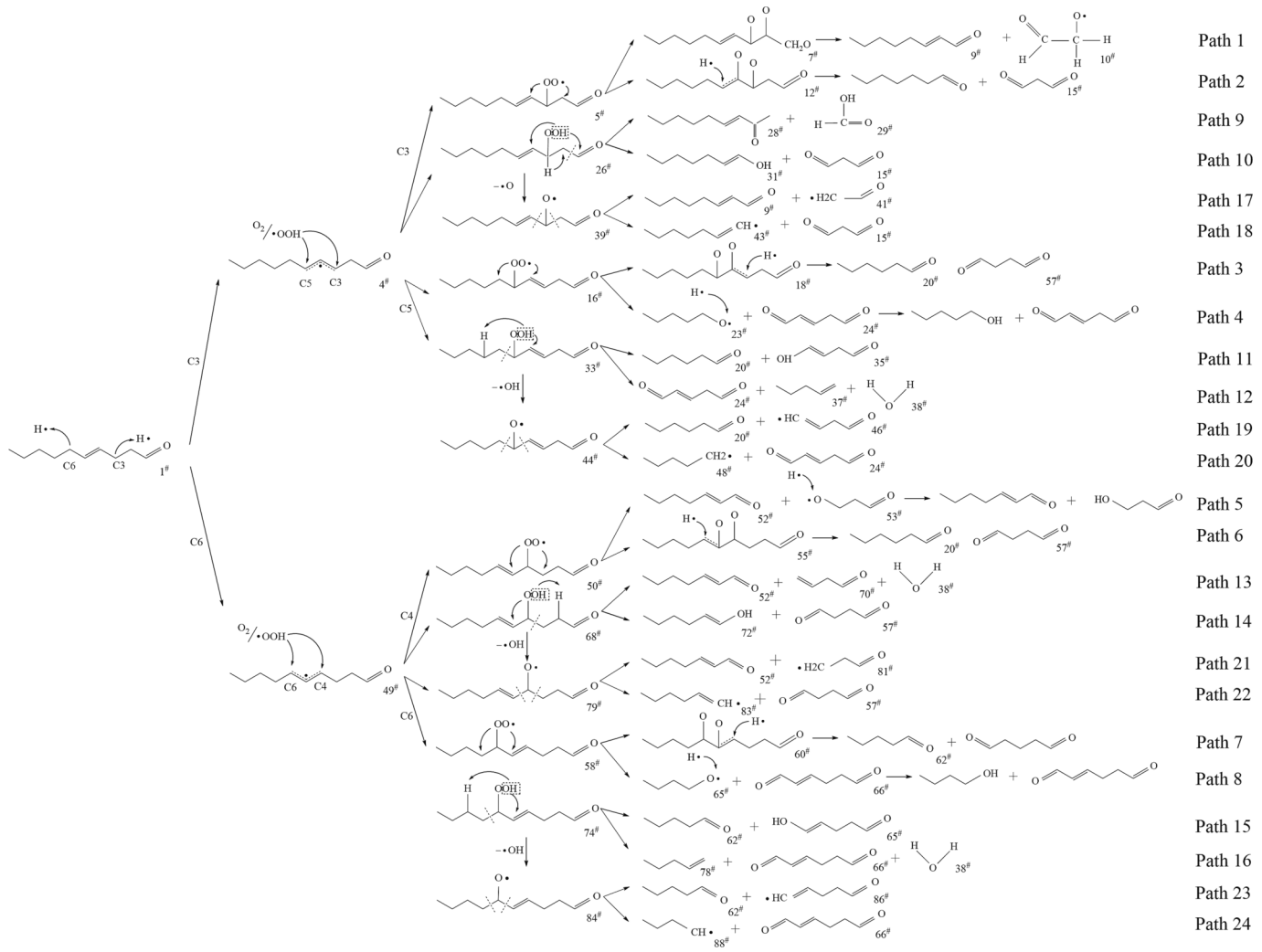

Fig. 4. Decomposition pathways of (E)-4-decenal thermal oxidation.

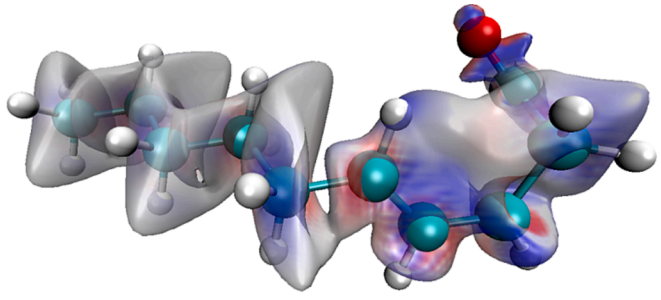

Fig. 5. Schematic diagram of the molecular orbital for the breaking of the C—H bond at C3.

TS69$^{\#}$ to form the end products: 2-heptenal, 3-butenone and hydrone (Path 13). Whereas if C5 is attacked, the adjacent C4-C5 bond will be broken directly via TS71$^{\#}$ to form the final products: (E)-2-hexen-1-ol and butanedione (57$^{\#}$&72$^{\#}$, Path 14). The 5-ROOH is further cleaved via transition state TS34$^{\#}$ to form the final products: hexanal and 3-butenal-4-ol (20$^{\#}$&35$^{\#}$, Path 11). Oxidative cleavage via TS36$^{\#}$ form glutaric dialdehyde, 1-butene and hydrone (24$^{\#}$& 37$^{\#}$&38$^{\#}$, Path 12). The 6-ROOH is cleaved via TS75$^{\#}$ to form the final products: pentanal and 4-pentenal-5-ol (62$^{\#}$&65$^{\#}$, Path 15), and cleavage via TS77$^{\#}$ gives the final products: butene, 2-adipaldehyde and hydrone (78$^{\#}$&66$^{\#}$&38$^{\#}$, Path 16).

Analysis of alkoxy radical reaction mechanism (RO·) in (E)-4-decenal thermal oxidation

As shown in the Fig. 2 and Fig. 4, after the formation of peroxides (26$^{\#}$, 33$^{\#}$, 68$^{\#}$, 74$^{\#}$), the structure can continue to absorb energy to break the O-OH bond in the peroxide to form 3-RO· (39$^{\#}$, R_{32}), 4-RO· (79$^{\#}$, R_{34}), 5-RO· (44$^{\#}$, R_{33}), 6-RO·(84$^{\#}$, R_{35}), respectively. These alkoxy radicals would continue to attack the adjacent carbon atom, which causes oxidative breakage of both sites of the alkoxy radicals. As shown in the Fig. 4 (Path 17 and Path 18), in the 3-RO· structure, the O· attacks and breaks C2-C3 bond after going through the TS40$^{\#}$ (R_{36}) to form hexanal and $CHOCH_2CH$· group (9$^{\#}$&41$^{\#}$, Path 17). Meanwhile, the O· attacks and breaks the C3-C4 bond directly via the TS42$^{\#}$ (R_{37}) to form the final product: 2-pentendialdehyde and $CH_3(CH_2)_3CH_2$· group (15$^{\#}$&43$^{\#}$, Path 18). Similarly, via the TS80$^{\#}$ (R40), C3-C4 bond gradually breaks to form the final products: 2-heptenal and $CHOCH_2CH_2$· group (52$^{\#}$&81$^{\#}$, Path 21). While the C4-C5 bond of the 4-RO· breaks via the the TS82$^{\#}$ (R_{41}), the final products: 2-butanedial and $CH_3(CH_2)_3CHCH$· group are formed (57$^{\#}$&83$^{\#}$, Path 22). 5-RO· could further oxidize via the TS45$^{\#}$(R_{38}) or TS47$^{\#}$(R_{39}) to form the products hexanal and $CHOCH_2CHCH$· group (20$^{\#}$&46$^{\#}$; Path 19) or 2-pentendialdehyde and $CH_3(CH_2)_2CH_2$· group (24$^{\#}$&48$^{\#}$; Path 20), respectively. 6-RO· would attack C5 or C7 site to form final products: pentanal and CHO $(CH_2)_2CHCH$· group (62$^{\#}$&86$^{\#}$; Path 23) or 2-hexendialdehyde and

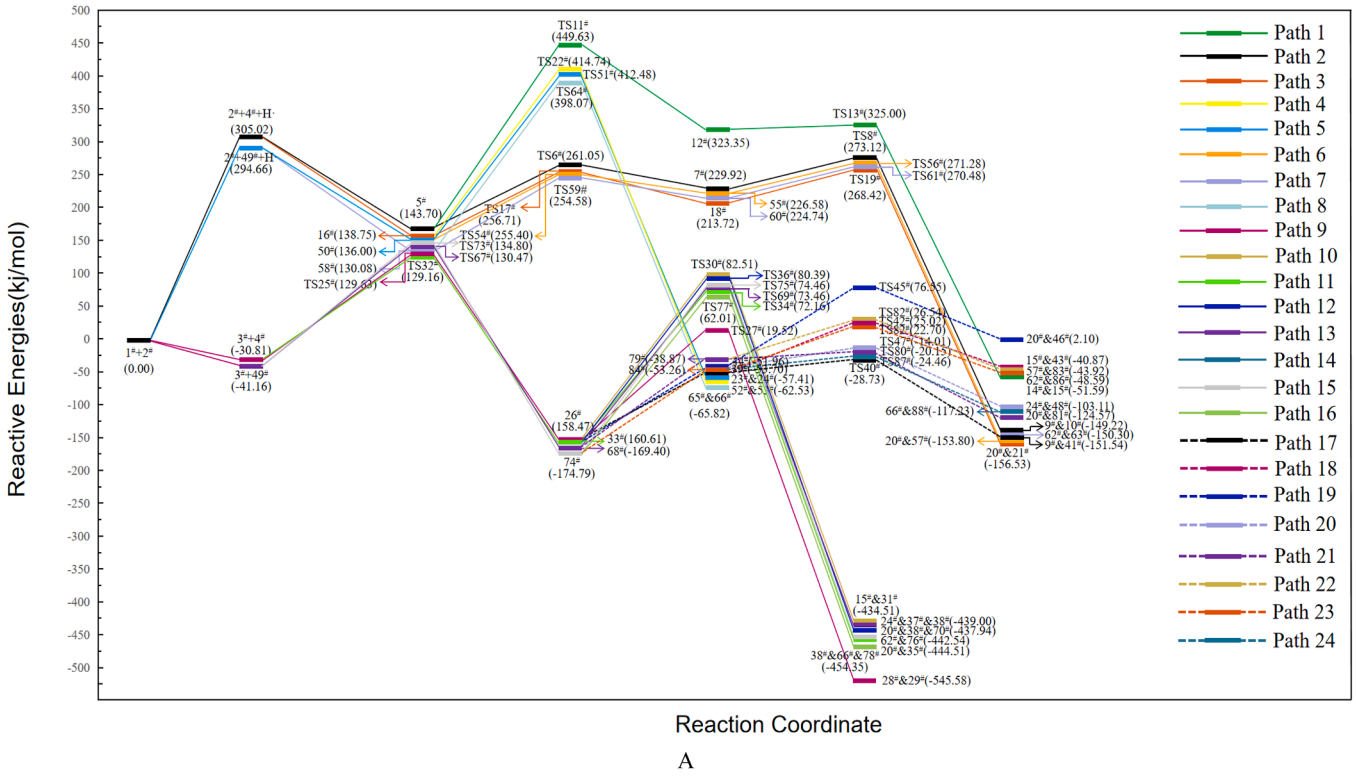

A

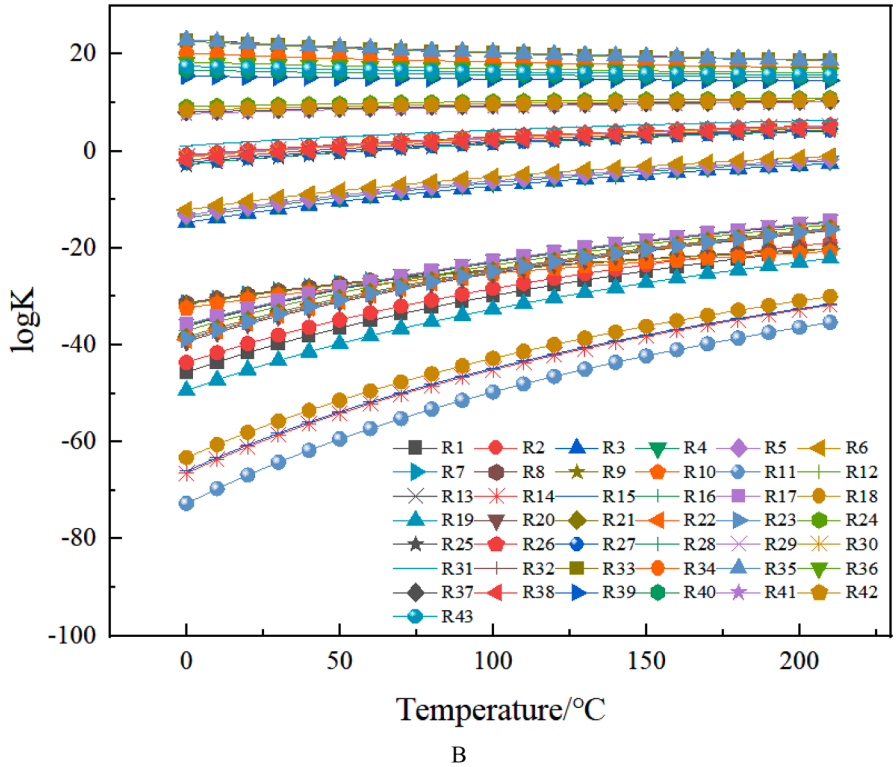

B

Fig. 6. Potential energy diagram with (E)-4-decenal oxidation reaction rate constants. (A) Potential energy diagram of (E)-4-decenal oxidation process. The value in brackets are the potential energy of the reaction at 298K. Each color line represents a chemical pathway. (B) The rate constant of various oxidation processes of (E)-4-decenal.

$CH_3(CH_2)_2CH\cdot$ group ($66^{\#}$&$88^{\#}$; Path 24) via the $TS85^{\#}(R_{42})$ or $TS87^{\#}(R_{43})$, respectively.

Analysis of the key reactions and priority of different mechanisms of (E)-4-decenal thermal oxidation

As shown in Fig. 2, compounds $5^{\#}$, $16^{\#}$, $26^{\#}$, $33^{\#}$, $39^{\#}$, $44^{\#}$, $50^{\#}$, $58^{\#}$, $68^{\#}$, $74^{\#}$, $79^{\#}$, and $84^{\#}$ are all located at the branching points in the

(E)-4-decenal oxidation reaction network, which means that these compounds determine the course of the subsequent oxidation reactions. Therefore, these compounds are considered as the key intermediates in the oxidation of the (E)-4-decenal. Meanwhile, the chemical reactions from the key intermediates are usually considered to be the key reactions in the reaction network. As a result, the reactions R_{11}–R_{18}, R_{24}–R_{32}, and R_{36}–R_{43} are considered to be the key chemical reactions in their reaction pathways.

Fig. 6(A) shows the energy barrier for the oxidation processes of (E)-4-decanal. Additionally, Fig. 6(B) shows the reaction rate constants for various oxidation reactions. The Tab. S1 contains information on each reaction rate constant at various temperatures. It is well acknowledged that a chemical reaction's energy potential barrier represents the bare minimal amount of energy needed to carry out the reaction. As a result, chemical reactions with high energy barriers are challenging to carry out. Reactions are easier to occur when potential barriers are smaller. It can be seen from Fig. 6(A) that the energy potential barriers for most of key reactions are higher than others in the reaction pathway of (E)-4-decenal. This phenomenon further confirms the conclusion that R_{11}-R_{18}, R_{24}-R_{32} and R_{36}-R_{43} are the key chemical reactions in their reaction pathways.

The energy required for reactions of peroxyl radical pathway range from 210 KJ/mol to 420 KJ/mol, as shown in Fig. 6(A), while the energy required for reactions of peroxide pathway range from 20 KJ/mol to 85 KJ/mol. It is obvious that the peroxyl radical reaction pathway has a substantially higher energy barrier than the peroxide reaction pathway. As a result, under the identical circumstances, the peroxide reaction route is easier to react. And the peroxide reaction pathway is preferred over the peroxyl radical reaction pathway. Meanwhile, it can be clearly seen from Fig. 6(A) that all of the reactions in the alkoxyl radical pathway require a lower barrier than that of the peroxide reaction pathway. It means that the alkoxyl radical reaction pathway is preferred over the peroxide reaction pathway. Furthermore, Fig. 6(B) shows that the alkoxy radical pathway's reaction rate constants are significantly larger than those of the other pathways. Additionally, most processes' reaction rate constants show a propensity to rise with temperature. Based on the results above, it can be concluded that in the (E)-4-decenal thermal oxidation process, the alkoxy radical reaction pathway has priority over the peroxide reaction pathway, and the peroxide pathway has priority over the peroxyl radical pathway.

In addition, the calculated reaction priority agrees well with the experimental results based on the fact that the products with higher potential energy barrier have higher formation temperatures than the lower ones in the experiment. For example, the typical products of Path 1 and Path 9 are (E)-2-octenal ($9^{\#}$) and 3-nonene-2-ketone ($28^{\#}$), respectively. The reaction barrier for the creation of 3-nonene-2-ketone ($28^{\#}$) is 129.63 KJ/mol (R_7), which is higher in the ROOH reaction pathway. In the experiment, it is found that this substance's formation temperature is likewise higher (150 °C). Similarly, (E)-2-octenal ($9^{\#}$) has an energy barrier of 325.00 KJ/mol (R_{19}). It means that it is more difficult for this reaction to occur than other reactions. The outcomes of the experiment revealed that this compound could be detected at 120 °C. It is further demonstrated that the computed findings and the experimental data agree well.

Conclusion

In the deep oxidation of lipids, (E)-4-decenal is a significant byproduct that can further oxidize to produce volatile flavors with shorter carbon chains. DFT calculations were used to obtain a total of 43 reactions with 24 reaction pathways in the thermal oxidation of (E)-4-decenal. These reactions were categorized into three reaction mechanisms: peroxide (ROOH), alkoxy radical (RO·), and peroxyl radical (ROO·). The outcomes of the DFT calculations and the experiment were generally in agreement. The priority order of these reaction mechanisms is RO· mechanism > ROOH mechanism > ROO· mechanism.

CRediT authorship contribution statement

Binchen Wang: Writing – original draft, Data curation. **Shaohua Dou:** Software. **Shang Wang:** Visualization, Software. **Yi Wang:** Writing – review & editing. **Sufang Zhang:** Supervision, Methodology. **Xinping Lin:** Data curation. **Yingxi Chen:** Formal analysis. **Chaofan Ji:** Methodology. **Yiwei Dai:** Formal analysis, Data curation. **Liang Dong:** Writing – review & editing, Supervision, Resources, Project administration.

Declaration of competing interest

The authors declare that they have no known competing financial interests or personal relationships that could have appeared to influence the work reported in this paper.

Data availability

The authors do not have permission to share data.

Acknowledgement

We thank the support of the National Natural Science Foundation of China (No. 31871760).

Appendix A. Supplementary data

Supplementary data to this article can be found online at https://doi.org/10.1016/j.fochx.2024.101174.

References

Albaugh, A., Boateng, H. A., Bradshaw, R. T., et al. (2016). Advanced Potential Energy Surfaces for Molecular Simulation. *The journal of physical chemistry, 120*(37), 9811–9832. https://doi.org/10.1021/acs.jpcb.6b06414

Al-Otaibi, J. S., Mahmoud, M. A. M., & Almuqrin, A. H. (2021). Ab initio-based kinetics of hydrogen atom abstraction from methyl propionate by h and ch3 radicals: A biodiesel model. *Structural Chemistry, 32*(5), 1857–1872. https://doi.org/10.1007/s11224-021-01746-6

Ama, A., Fb, A., Db, B., et al. (2019). RIFM fragrance ingredient safety assessment, 1-octen-3-ol, CAS registry number 3391–86-4-ScienceDirect. *Food and Chemical Toxicology, 134*. https://doi.org/10.1016/j.fct.2019.110972

Angela, K., & Andreas, M. (2010). Oxidation of unsaturated fatty acid derivatives and vegetable oils. *European Journal of Lipid Science & Technology, 110*(9), 812–824. https://doi.org/10.1002/ejlt.200800042

Balan, R. C., & Rajakumar, B. (2018). Photo oxidation reaction kinetics of ethyl propionate with cl atom and formation of propionic acid. *The Journal of Physical Chemistry A, 122*, 42. https://doi.org/10.1021/acs.jpca.8b05215

Becke, A. D. (1992). Density-functional thermochemistry. 1. The effect of the exchange-only gradient correction. *Journal of Chemical Physics, 96*, 2155–2160. https://doi.org/10.1063/1.462066

Becke, A. D. (1993). Density-functional thermochemistry. 3. The role of exact exchange. *Journal of Chemical Physics, 98*, 5648–5652. https://doi.org/10.1063/1.464913

Borges, R. M., Colby, S. M., Das, S., et al. (2021). Quantum chemistry calculations for metabolomics. *Chemical Reviews, 10*, 121. https://doi.org/10.1021/acs.chemrev.0c00901

Calín-Sánchez, Á., & Carbonell-Barrachina, Á. A. (2021). Flavor and aroma analysis as a tool for quality control of foods. *Foods, 10*, 224. https://doi.org/10.3390/foods10020224

Chai, D., Li, C. W., Zhang, X. X., et al. (2019). Analysis of volatile compounds from wheat flour in the heating process. *International Journal of Food Engineering, 15*(10), 1–13. https://doi.org/10.1515/ijfe-2019-0252

Charles, T., & Sebens.. (2021). Electron charge density: A clue from quantum chemistry for quantum foundations. *Foundations of Physics, 51*, 75. https://doi.org/10.1007/s10701-021-00480-7

Drabova, L., Tomaniova, M., Kalachova, K., et al. (2013). Application of solid phase extraction and two-dimensional gas chromatography coupled with time-of-flight mass spectrometry for fast analysis of polycyclic aromatic hydrocarbons in vegetable oils. *Food Control, 33*(2), 489–497. https://doi.org/10.1016/j.foodcont.2013.03.018

Dymerski, T. (2017). Two-dimensional gas chromatography coupled with mass spectrometry in food analysis. *Critical Reviews in Analytical Chemistry*. https://doi.org/10.1080/10408347.2017.1411248

Elroby, S. A., Banaser, B. A., Aziz, S. G., et al. (2022). Zn^{2+}-schiff's base complex as an "on-off-on" molecular switch and a fluorescence probe for Cu^{2+} and Ag^{+} ions. *Journal of Fluorescence, 32*(2), 691–705. https://doi.org/10.1007/s10895-021-02864-4

Frankel, E. N. (1983). Volatile lipid oxidation products. *Progress in Lipid Research, 22*(1), 1–33. https://doi.org/10.1016/0163-7827(83)90002-4

Fukui, K. (1981). The path of chemical reactions-The IRC approach. *Accounts of Chemical Research, 14*, 12. https://doi.org/10.1021/ar00072a001

Grambow, C., Pattanaik, L., & Green, W. H. (2020). Reactants, products, and transition states of elementary chemical reactions based on quantum. *Chemistry, 7*, 137. https://doi.org/10.1038/s41597-020-0460-4

Hammes-Schiffer, S. (2017). A conundrum for density functional theory: DFT studies may sometimes get the right results for the wrong reasons. *Science, 355*(6320), 28–29. https://doi.org/10.1126/science.aal3442

Hine Nicholas, D., & Hine, N. D. M. (2016). Applications of large-scale density functional theory in biology. *Journal of Physics Condensed Matter, 28*, Article 393001. https://doi.org/10.1088/0953-8984/28/39/393001

Humphrey, W. F., Dalke, A., & Schulten, K. (1996). VMD: Visual molecular dynamics. *Journal of Molecular Graphics, 14*(1), 33–38. https://doi.org/10.1016/0263-7855(96)00018-5

Jeleń, H. H., Majcher, M., & Dziadas, M. (2012). Microextraction techniques in the analysis of food flavor compounds: A review. *Analytica Chimica Acta, 738*, 13. https://doi.org/10.1016/j.aca.2012.06.006

Li, X., & Josef, P. (1996). Valence bond description of spin properties of π-conjugated systems. *Chemical Physics, 204*(2–3), 447–461. https://doi.org/10.1016/0301-0104(95)00291-X

Mahmoud, M., Shiroudi, A., & Abdel-Rahman, M. A. (2020). Structures, energetics, and kinetics of h-atom abstraction from methyl propionate by molecular oxygen: Ab initio and dft investigations. *Computational and Theoretical Chemistry, 1196*, 2. https://doi.org/10.1016/j.comptc.2020.113119

Peng, C.-Y., Lan, C. H., Lin, P. C., et al. (2017). Effects of cooking method, cooking oil, and food type on aldehyde emissions in cooking oil fumes. *Journal of Hazardous Materials, 324*, 160. https://doi.org/10.1016/j.jhazmat.2016.10.045

Peter, Q. T., Giorgia, P., Mariarosa, M., et al. (2016). Impact of comprehensive two-dimensional gas chromatography with mass spectrometry on food analysis. *Journal of Separation Science*. https://doi.org/10.1002/jssc.201500379

Porter, N. A., Caldwell, S., & Mills, K. A. (1995). Mechanisms of free radical oxidation of unsaturated lipids. *Lipids, 30*, 4. https://doi.org/10.1007/BF02536034

Ryu, H.o., Park, J. Y., & KiM, H. K. (2018). Pitfalls in computational modeling of chemical reactions and how to avoid them. *Section B: Structure Science Crystal Engineering Materials*, 171–179. https://doi.org/10.1021/acs.organomet.8b00456

Ryu, H., Park, J., Kim, H. K., et al. (2018). Pitfalls in computational modeling of chemical reactions and how to avoid them. *Organometallics, 37*(19), 3228–3239. https://doi.org/10.1021/acs.organomet.8b00456

Santacesaria, E., Sorrentino, A., Rainone, F., et al. (2000). Oxidative cleavage of the double bond of monoenic fatty chains in two steps: A new promising route to azelaic acid and other industrial products[J]. *Industrial & Engineering Chemistry Research, 39*(8), 2766–2771. https://doi.org/10.1021/ie990920u

Shabani, M., Latina, J., & Li, Z. (2020). Comparison of ultra-high-resolution with conventional ct-derived coronary lumen visibility in patients with coronary artery disease. *Journal of Cardiovascular Computed Tomography, 14*(3), 541. https://doi.org/10.1016/j.jcct.2020.06.063

Sheridan, J. (1946). Mechanisms of reactions at carbon-carbon double bond. *Interscience Publishers, 161*, 626. https://doi.org/10.1016/j.jhazmat.2016.10.045

Stier, R. F. (2000). Chemistry of frying and optimization of deep-fat fried food flavour-An introductory review. *European Journal of Lipid Science & Technology, 102*(8–9), 507–514. https://doi.org/10.1002/1438-9312(200009)102:8/9<507::AID-EJLT507>3.0.CO;2-V

Tian, L., & Chen, F. (2012). Multiwfn: A multifunctional wavefunction analyzer. *Journal of Computational Chemistry, 33*(5), 580–592. https://doi.org/10.1002/jcc.22885

Tian, L., & Chen, Q. H. (2021). Shermo: A general code for calculating molecular thermochemistry properties. *Computational and Theoretical, Chemistry, 1200*, 113249. https://doi.org/10.1016/j.comptc.2021.113249

Verma, P., & Truhlar, D. G. (2020). Status and challenges of density functional theory. *Trends Chemistry, 2*(4). https://doi.org/10.1016/j.trechm.2020.02.005

Yang, P., & Lee.. (1986). Various functionals for the kinetic energy density of an atom or molecule. *Physical Review. A, General Physics, 34*, 6. https://doi.org/10.1103/physreva.34.4586

Wang, B., Zhang, S., Lin, X., et al. (2023). Deep exploration of lipid oxidation into flavor compounds: a density functional theory study on (E)-2-decenal thermal oxidative reaction. *FoodChemistry, 428*. https://doi.org/10.1016/j.foodchem.2023.136725

Zaldman, B., Klsillev, A., & Sasson, Y. (1988). Double bond oxidation of unsaturated fatty acids. *Journal of the American Oil Chemists' Society, 65*(4), 611–615. https://doi.org/10.1007/BF02540689